S. Y. ZAMRIK*, D. J. LEDGER* and C. DATÉ**

Fatigue Characteristics of Thin Titanium Plates Due to Biaxial Stress Cycling

* The Pennsylvania State University, University Park, Pa, 16802, USA
** Allied-Signal Aerospace Co., Phoenix, AZ, 85010, USA

Keywords: Biaxial Fatigue, Fracture, Crack Growth, Thin Plate Specimens, Anticlastic Bending

ABSTRACT: The paper discusses the fatigue characteristics in thin Titanium plate specimens of rhombic configuration. Specimens were subjected to biaxial stress field using the anticlastic bending method where two bending moments are developed. The anticlastic bending method generates two surfaces of curvatures: one surface in tension while the other in compression resulting in negative biaxial stress ratio.

Fatigue data resulting from a number of biaxial stress ratios were obtained and the results were analyzed using yield theories as well as stress intensity factor. The stress intensity factor approach was used to characterize the failure mode.

Notation

δ	total deflection of plate
ε_1	in-plane principal strain in x-direction
ε_2	in-plane principal strain in y-direction
ν	Poisson's ratio
ϕ_σ	biaxial stress ratio
ϕ_ε	biaxial strain ratio
σ_1	in-plane principal stress in x-direction
σ_2	in-plane principal stress in y-direction
σ_Y	uniaxial material tensile yield stress
a	half the length of diagonal BC (along minor axis)
b	half the length of diagonal AD (along major axis)
c	distance from diagonal BC
E	elastic modulus
F	load applied at each corner
M_L	bending moment per unit length
N_f	cycles to failure
P_y	yield load
t	plate thickness

Introduction

Numerous engineering structures are subjected to cyclic biaxial stresses as in pressure vessels and nozzles, turbine blades, and sheet materials with complex geometry. In the early 1950's, the Pressure Vessel Research Committee initiated a research program to study the effect of biaxial stress cycling on the fatigue life of pressure vessels in order to improve material selection and fabrication processes, Tor [1].

A number of experimental methods to generate a biaxial state of stress/strain were developed over the years such as tubular specimens subjected to cyclic pressure, tension-torsion, oval plates subjected to cyclic pressure, cruciform specimens subjected to tension-tension or tension-compression, cantilever bending specimens, and the anticlastic plate bending method. Each method has its advantages and disadvantages which can be found in the literature. From the viewpoint of economy and ease in conducting biaxial fatigue testing, reverse bending of plate specimen has a great advantage over other methods. However, from an academic point of view, there are several advantages for using combined axial-torsion (biaxial) fatigue testing with thin-walled cylindrical specimens which practically eliminate the influence of through-thickness stress-strain gradients. Also, the stress-strain responses in low cycle fatigue tests can be measured directly from the hysteresis loop; whereas in plate bending there are some ambiguities in the computation of the plastic strain range from the total strain range and load measured in low cycle fatigue testing. However, if the criterion for fatigue failure is crack initiation or growth of a surface crack to a certain length, then this disadvantage can be tolerated to some extent because the primary interest becomes the influence of the biaxial stress state on crack initiation or growth rather than to determine the absolute values of low cycle fatigue life under various states of biaxial stresses.

The Anticlastic Bending Method

A unique feature of the anticlastic bending method when applied to the rhombic plate design is the uniform stress and strain distribution over a wide area of the specimen surface. This is because the rhombic plate can be assumed to be constituted of beams of uniform strength along its two diagonals by a simple beam theory approximation, whereas, for both the wide-cantilever beam and the pressured-plate specimens, only a limited area

in the central portion of either specimen is subject to the maximum stress or strain state. As a comparison to the pressured-plate techniques, the anticlastic bending of a rhombic plate method is more convenient for detecting and observing the initiation and growth of cracks on the surface of the specimen. The fact that the stress-strain distribution over the rhombic plate surface is uniform under cyclic loading also provides an advantage in easily obtaining the magnitude of the stresses and strains at the specimen surfaces. Even though there is a continuous change in the stress-strain relation for the material as the number of cycles increases, the varying stress-strain relation is the same over the entire surface of the rhombic plate. Therefore, the strain-deflection relation at the beginning of the test remains unchanged throughout the test as far as the assumption of linear distribution of strain in the direction of the thickness holds; hence, once the strain-deflection relation is initially calibrated, before testing begins, the only required measurement needed during the testing is the deflection of the plate.

Basically, the plate specimen has a rhombic geometry where the surface, when subjected to anticlastic bending, undergoes a tension-compression mode resulting in bending moments of opposite sign are generated from a central load. The centrally applied load P generated loads F at the corners of the plate (Figure 1).

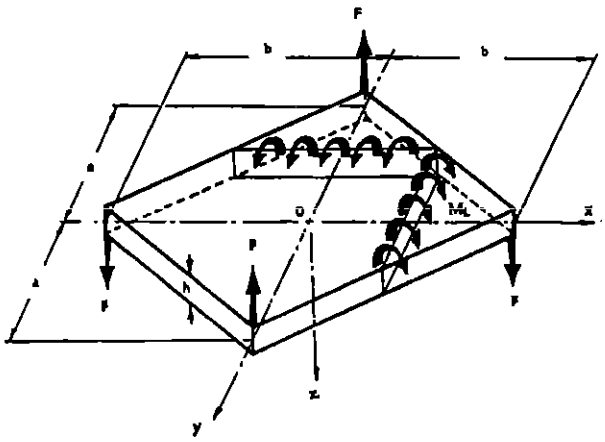

Fig. 1 Schematic of rhombic plate specimen loading configuration in anticlastic bending mode

As a result of this type of loading, bending stresses are generated on the surfaces of the plate which are proportional to the radii of curvature. The stress or strain ratio can be varied by changing the length of the diagonals resulting in a wide range of stress or strain

ratios. In theory, principal stress ratios from 1:-1 to 1:0 or 2:1 and principal strain ratios from 1:-1 to 2:-1 or 1:0 can be achieved and can be compared to other state of stress developed by other methods as shown in Figure 2. A schematic diagram of the apparatus is shown in Figure 3. Detail of the system and its construction can be found in ASTM publication Zamrik and Davis [2].

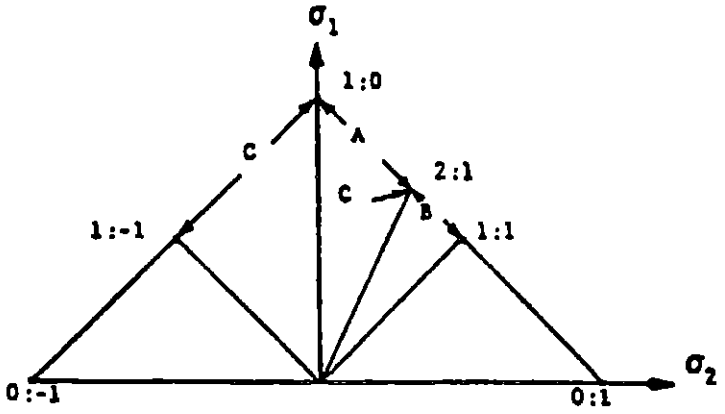

Fig. 2a Stress ratios attained by (A) Wide-Cantilever Beam, (B) Pressurized Oval Plates, (C) Anticlastic Bending

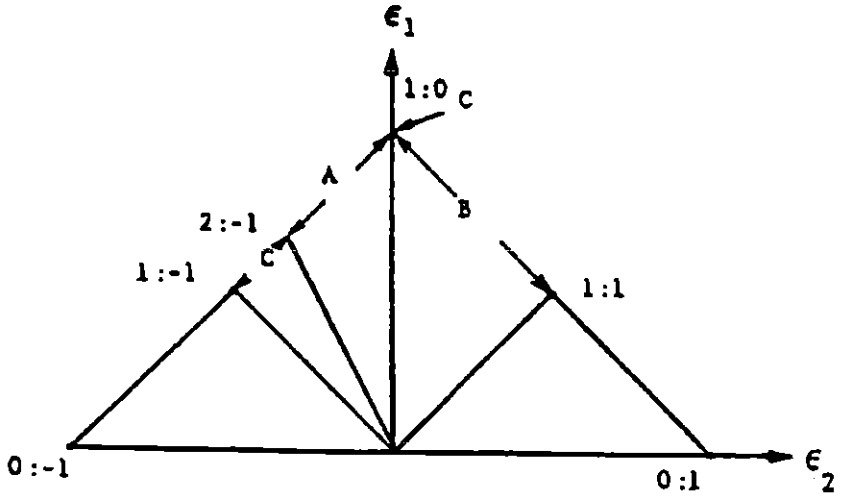

Fig. 2b Strain ratios attained by: (A) Wide-Cantilever Beam, (B) Pressurized Oval Plates, (C) Anticlastic Bending

(1M) Holder on moving die
(1S) Holder on stationary die
(2) Shelter
(3) Roller
(4) Rubber pin
(5) Connector to moving die
(6) Connector to stationary die

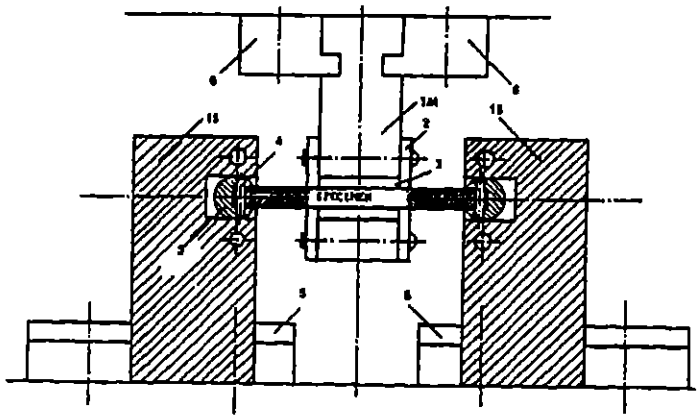

Fig. 3 Cross-Sectional view of anticlastic bending apparatus

Material and Rhombic Specimen

Titanium alloy type 6Al-2Sn-4Zr-2Mo forged plate material was used to fabricate plate specimens having a nominal thickness of 0.20 in (0.50 cm) and diagonals of 3x3 in (7.6x7.6 cm), 3x2 in (7.6x5.0 cm) and 3x1.5 in (7.6x3.8 cm). This type of geometry, as shown in Figure 4, generates principal minimum stress/maximum stress ratios of -1.0, -0.44 and -0.25 and a principal minimum strain/maximum strain ratios of -1.0, -0.68, and -0.54 respectively. The material mechanical properties are given in Table 1.

Table 1 Uniaxial Tensile Mechanical Properties of Ti-6242

Yield Stress (0.2% offset)	937 MPa	(136 Ksi)
Ultimate Strength	1010.7 MPa	(146.5 Ksi)
Modulus of Elasticity	124 GPa	($18x10^6$ psi)
Poisson's Ratio	0.34	
Percent Elongation	14.6%	

minor axis	a in(cm)	1.5 (3.8)	1 (2.54)	0.75 (1.9)
major axis	b in(cm)	1.5 (3.8)	1.5 (3.8)	1.5 (3.8)

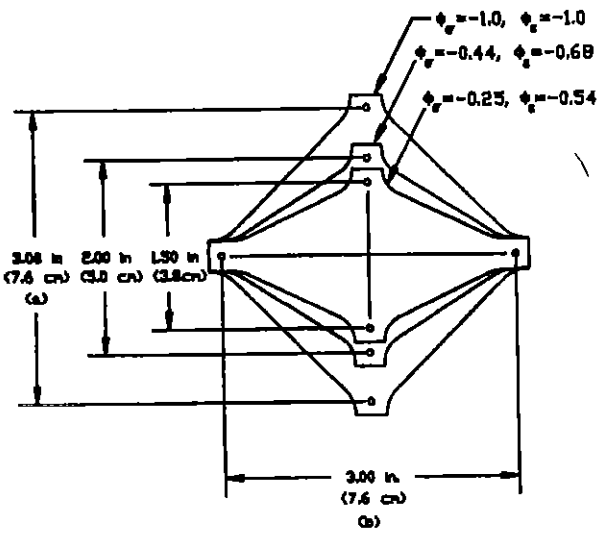

Fig. 4 Rhombic plate specimens with corresponding stress and strain ratios

Fatigue Test Procedure

The titanium rhombic plate specimens were cycled under stroke control from zero to maximum load using a triangular wave at a frequency of 2.0 Hz. Failure was defined by a 10% drop in the load from its maximum magnitude. A three-element rosette strain gage was placed at the center of the plate specimens and single element strain gages were placed along the major and minor axis of the plates as shown in Figure 5.

Similar gages were placed at the corresponding bottom surface. The gages were used for calibration and strain measurements at the top and bottom surfaces. Typical calibration is shown in Figure 6.

A total of 16 specimens were fatigue tested. Three specimens of 3x3 in (7.6x7.6 cm) were tested under load control and the remaining 13 specimens under stroke control. At the same maximum load, fatigue lives for the 3x3 in (7.6x7.6 cm) specimens were nearly identical for stroke and load control tests.

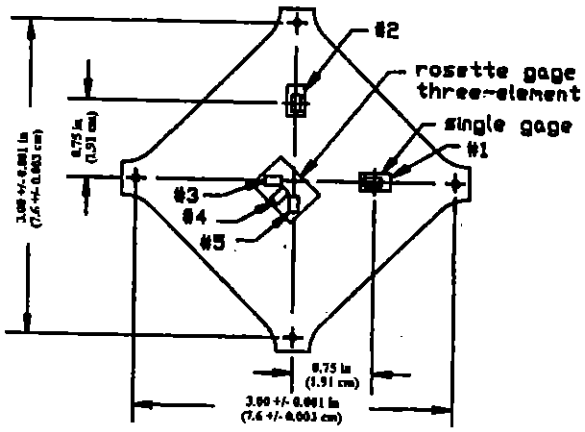

Fig. 5 Drawing of 3x3 in (7.6x7.6 cm) rhombic plate specimen with mounted top strain gages

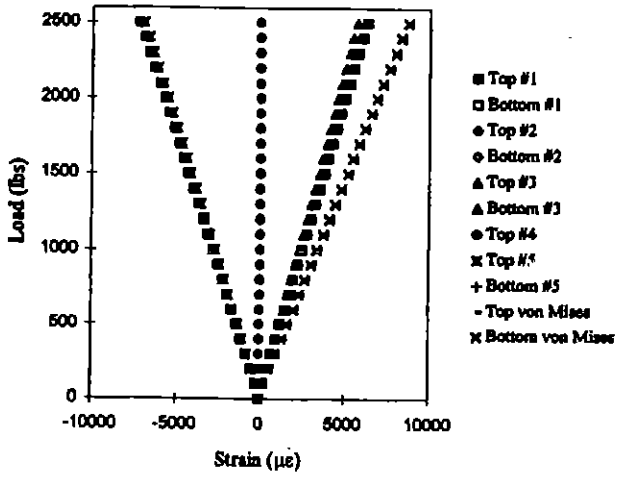

Fig. 6 Load (lbs) versus Strain (με) of specimen 3x3 in (7.6 x 7.6 cm)

Yield Loads and Stress/Strain Biaxiality Ratios

The yield load for the various plate specimens configurations were determined using Hooke's law assuming plane stress condition. For the specimen geometry, loading by a central force P as shown in Figure 7, the bending moment per unit length , M_L, along line segment JK, a distance c from diagonal BC, is a function of the resulting corner load F:

$$M_L = F\,(b\text{-}c) / L \qquad (1)$$

where F = load applied at each corner

b = half the length of diagonal AD (along major axis)

a = half the length of diagonal BC (along minor axis)

c = distance from diagonal BC

For the 3x3 in (7.6x7.6 cm) specimen and from similar triangle:

$$L = 2(b\text{-}c)\ (a/b) \qquad (2)$$

Substituting Equation (2) into (1):

$$M_L = (F/2)\ (b/a) \qquad (3)$$

and from symmetry, the total external centrally applied load P = 2F, hence:

$$M_L = (P/4)\ (b/a) \qquad (4)$$

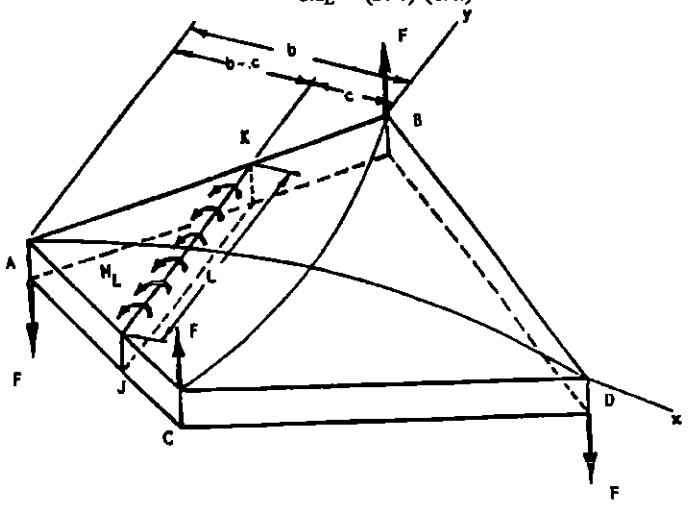

Fig. 7 Rhombic plate under anticlastic bending.

Since M_L is independent of the distance c, and constant along line segment JK, it is now called M_1 resulting in a bending stress:

$$\sigma_1 = 6\,M_1 / t^2 \qquad (5)$$

The stress can also be expressed in terms of the applied load P:

$$\sigma_1 = 3P/2\,t^2 \qquad (6)$$

For a biaxial state of stress, the von Mises failure criterion on the basis of yield condition is:

$$\sigma_1^2 + \sigma_2^2 - \sigma_1 \sigma_2 = \sigma_y^2 \quad (7)$$

or in terms of stress ratio $\phi_\sigma = \sigma_2 / \sigma_1$:

$$\sigma_1^2 (1 + \phi_\sigma^2 - \phi_\sigma) = \sigma_Y^2 \quad (8)$$

where σ_1 and σ_2 are applied in the x and y directions.

The stress ratio ϕ_σ is also a function of the diagonals a and b and has the form of (a^2/b^2).

By setting $P = P_Y$, the yield load is expressed as:

$$P_Y = 2 t^2 \sigma_Y \ / \ [3 (1+ \phi_\sigma^2 - \phi_\sigma)^{1/2}] \quad (9)$$

and for the 3x3 in (7.6x7.6 cm) specimen, setting $\phi_\sigma = -1$:

$$P_Y = 2 t^2 \sigma_Y / [3 (3)^{1/2}] \quad (10)$$

Expressions for the yield loads for the 3x2 in (7.6x5.0 cm) and 3x1.5 in (7.6x3.8 cm) specimens were similarly derived and presented in Table 2 and Table 3 for the biaxial stress and strain ratios.

Deflection-load relations for the 3x3 in (7.6x7.6 cm) specimen were derived from plate theory resulting in :

$$\delta = P b^2 (1- \upsilon \phi_\sigma) / 4 D (1 - \upsilon^2) \quad (11)$$

and for the 3x2 in (7.6x5.0 cm) specimen:

$$\delta = 3 P b^2 (1- \upsilon \phi_\sigma) / 8 D (1 - \upsilon^2) \quad (12)$$

and for the 3x1.5 in (7.6x3.8 cm) specimen:

$$\delta = 6 P b^2 (1- \upsilon \phi_\sigma) / 2D (1 - \upsilon^2) \quad (13)$$

where $D = Et^3 / 12 (1 - \upsilon^2)$

Table 2 Yield Load for each Rhombic Plate Configuration

Specimen		Thickness, t		$\phi_\sigma = (a^2/b^2)$	P_Y	
(cm)	(in)	(cm)	(in)		(N)	(lb)
7.6x7.6	(3x3)	0.5	(0.20)	-1.0	9314	(2094)
7.6x5.0	(3x2)	0.5	(0.20)	-0.44	8398	(1888)
7.6x3.8	(3x1.5)	0.5	(0.20)	-0.25	7041	(1583)

Table 3 Biaxial Stress and Strain Ratios for Rhombic Plate Specimens

Specimen		ϕ_σ	ϕ_ε
(cm)	(in)		
7.6x7.6	(3x3)	-1.0	-1.0
7.6x5.0	(3x2)	-0.44	-0.68
7.6x3.8	(3x1.5)	-0.25	-0.54

The surface strain for the 3x3 in (7.6x7.6 cm) specimen in terms of stress ratio :

$$\varepsilon_1 = (1/E) [\, 1 - \upsilon \phi_\sigma \,] \sigma_1 \quad (14)$$

$$\varepsilon_2 = (1/E) [\, \phi_\sigma - \upsilon \,] \sigma_1 \quad (15)$$

or in term of the applied load P:

$$\varepsilon_1 = (3\,P / 2\,E\,t^2) [\, 1 - \upsilon \phi_\sigma \,] \quad (16)$$

$$\varepsilon_2 = (3\,P / 2\,E\,t^2) [\, \phi_\sigma - \upsilon \,] \quad (17)$$

and the third principal strain is expressed in terms of the biaxial strain ratio, $\phi_\varepsilon = \varepsilon_2 / \varepsilon_1$:

$$\varepsilon_3 = -[\upsilon / (1 - \upsilon)] [\, 1 + \phi_\varepsilon \,] \varepsilon_1 \quad (18)$$

Similar derivation for strain-deflection-load expressions were derived for the 3x2 in (7.6x5.0 cm) and 3x1.5 in (7.6x3.8 cm) specimens.

Test Results

Biaxial fatigue test results from the 3x3 in (7.6x7.6 cm), 3x2 in (7.6x5.0 cm), and 3x1.5 in (7.6x3.8 cm) rhombic plate series were plotted in terms of maximum shear strain, maximum principal strain and von Mises effective strain versus number of cycles to failure as shown in Figures 8, 9 and 10 on semi-log plots to show the scatter in the data. Although the scatter band is wider than desired, the von Mises has shown a better correlation for plate bending with a scatter of ± 2.7x, whereas the maximum shear strain scatter was ± 4.2x and the maximum principal strain was ± 3.5x.

Failure Modes

Typical failure modes are presented for the three types of the specimen's geometry. Specimen 3x3 under load control was cycled to a maximum load of 2,200 lb (9,785 N) with a maximum tensile strain of 0.56 %. Two crack initiation sites were observed on the top surface in quadrant II (tension side), which then joined to form a larger crack propagating perpendicular to the maximum principal tensile stress direction as shown in Figure 11a. Figure 11b shows the initiation sites and fatigue beach marks. The cycles to failure were 592,248.

For specimen 3x2 in (7.6x5.0 cm) which was cycled under stroke control to a maximum load of 2,500 lb (11,120 N), 612 lb (2,722 N) above the yield and with a maximum principal tensile strain of 0.84%, two crack initiation sites were also observed. Crack propagation was in Mode I as shown in Figure 12. Cycles to failure were 46,521.
For specimen type 3x1.5 in (7.6x3.8 cm) which was cycled under stroke control at a maximum load of 1600 lb (7,117 N), corresponding to 67 lb (298 N) above the yield. The maximum tensile strain was 0.72%. The fatigue crack initiated was in quadrant IV as shown in Figure 13. The cycles to failure were 90,549.

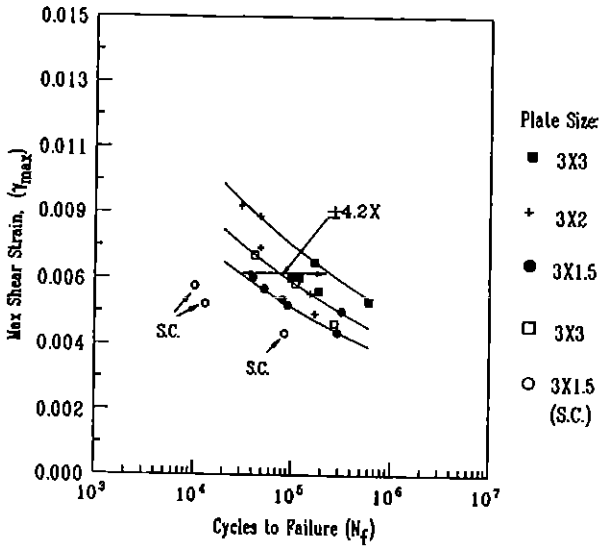

Fig. 8 Max Shear Strain versus Cycles to Failure for 3x3in (7.6x7.6 cm), 3x2in (7.6x5.0 cm), x1.5in (7.6x3.8 cm) S.C. = Crack Initiation at Stress Concentrators
Best Fit: $\gamma_{max} = 0.034N^{-0.148}$
Upper Scatter Band: $\gamma_{max} = 0.041N^{-0.148}$
Lower Scatter Band: $\gamma_{max} = 0.030N^{-0.148}$

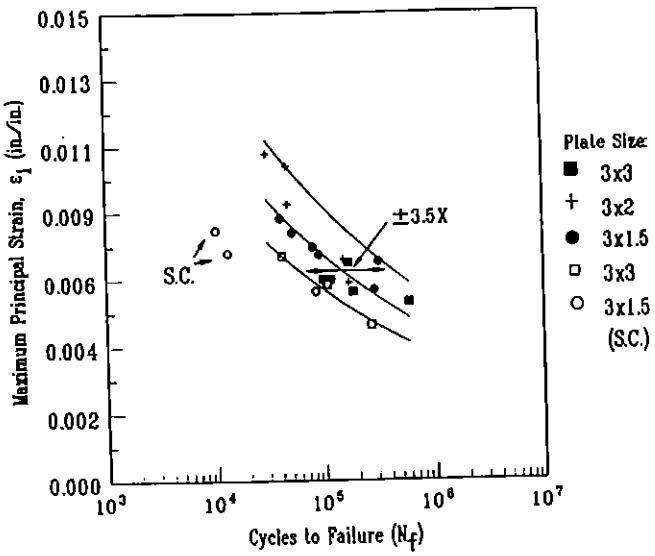

Fig. 9 Maximum Principal Strain versus Cycles to Failure for 3x3in (7.6x7.6 cm), 3x2in (7.6x5.0 cm), 3x1.5in (7.6x3.8 cm). S.C. = Crack Initiation at Stress Concentrators.
Best Fit: $\varepsilon_1 = 0.0607N^{-0.185}$
Upper Scatter Band: $\varepsilon_1 = 0.051N^{-0.185}$
Lower Scatter Band: $\varepsilon_1 = 0.0735N^{-0.185}$

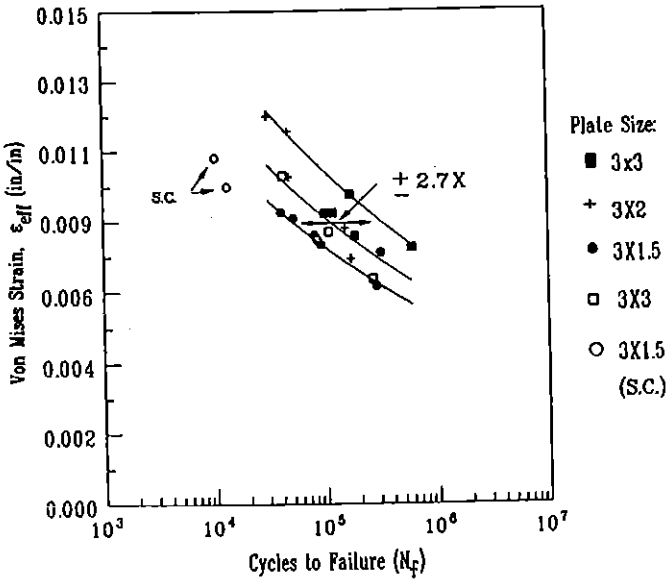

Fig. 10 Von Mises Strain versus Cycles to Failure for 3x3in (7.6x7.6 cm), 3x2in (7.6x5.0 cm), 3x1.5in (7.6x3.8 cm). S.C. = Crack Initiation at Stress Concentrators.
Best Fit: $\varepsilon_{eff} = 0.044N^{-0.1425}$
Upper Scatter Band: $\varepsilon_{eff} = 0.052N^{-0.1425}$
Lower Scatter Band: $\varepsilon_{eff} = 0.040N^{-0.1425}$

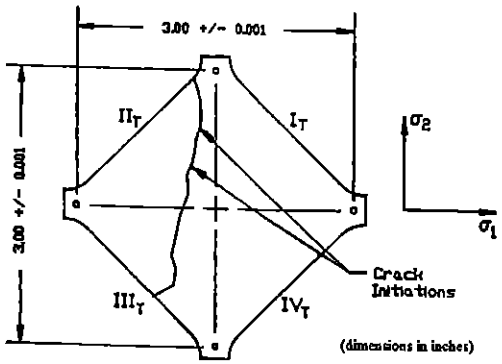

Fig. 11a Fatigue crack initiations on failure surface of plate spec. 3x3 in (7.6x7.6 cm), ϕ_σ 1.0, ϕ_ε = -1.0, ε_{max} = 0.56%, P_{max} = 9785 N, N_f = 592,248 cycles

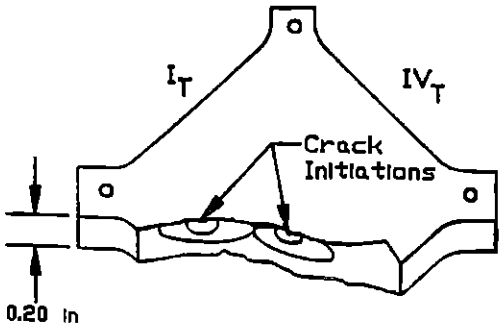

Fig. 11b Sketch of fracture surface with beach marks, specimen 3X3 in (7.6x7.6 cm)

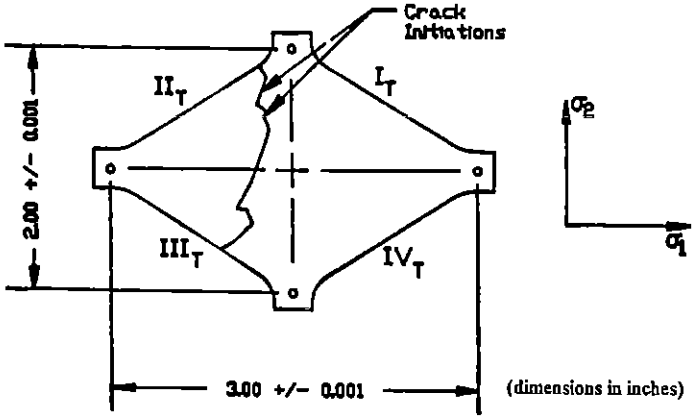

Fig. 12a Fatigue crack initiation sites, plate specimen 3x2 in (7.6x5.0 cm), ϕ_σ = -0.444, ϕ_ε = -0.68, ε_{max} = 0.84%, P_{max} = 2500 lb (11120 N), N_f = 46,521 cycles

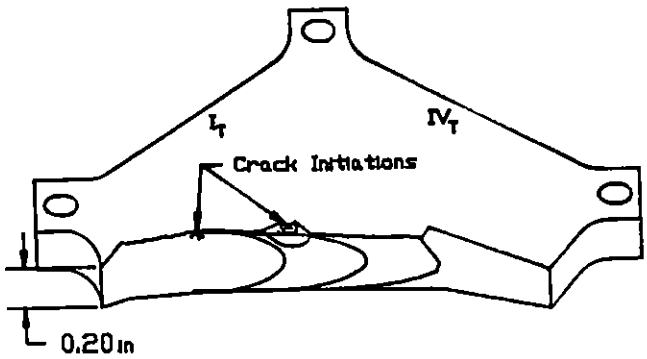

Fig. 12b Fracture surface with initiations, plate specimen 3x2 in (7.6x5.0 cm)

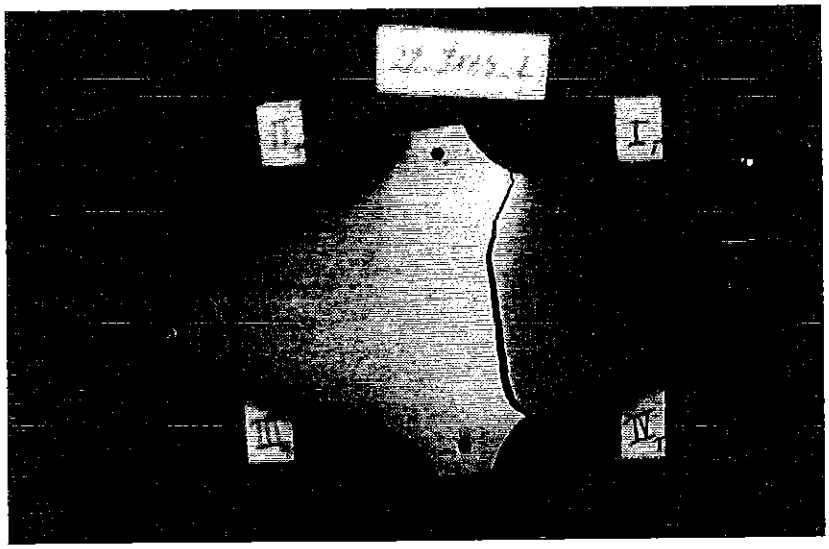

Fig. 13a Photograph of top of failure surface of plate specimen 3x1.5 in (7.6x3.8 cm)
$\phi_\sigma = -0.25$, $\phi_\varepsilon = -0.54$, $\varepsilon_{max} = 0.72\%$, $P_{max} = 1650$ lb (7339 N), $N_f = 90{,}549$ cycles

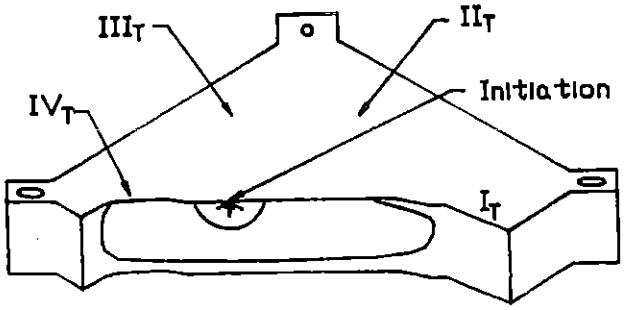

Fig. 13b Fracture surface with initiation site, specimen 3x1.5 in (7.6x3.8 cm)

Microstructure Analysis

The fracture behavior of the titanium plates was analyzed using a scanning electron microscope (SEM) and an optical microscope. Representative specimens from each series of plates were examined for important fracture features such initiation sites, and fracture mechanisms. Stress intensity ranges, ΔK, were calculated at various flaw depths using a modified analytical expression developed by Zamrik and Shabara [3] for biaxial bending. ΔKs were then related to the fracture behavior.

Figure 14 shows the fracture surface for a 3x3 in (7.6x7.6 cm) specimen tested at a maximum load of 2,600 lb (11,654 N) and a yield load of 2,093 lb (9,314 N). It also shows river markings emanating from the initiation sites. The fracture topology is characterized by transgranular facets intermixed with tear ridges and some secondary cracking where the flaw depth, a, was 0.002 in (0.005 cm), resulting in $\Delta K = 7$ Ksi$\sqrt{in}$ (8 MPa$\sqrt{m}$).

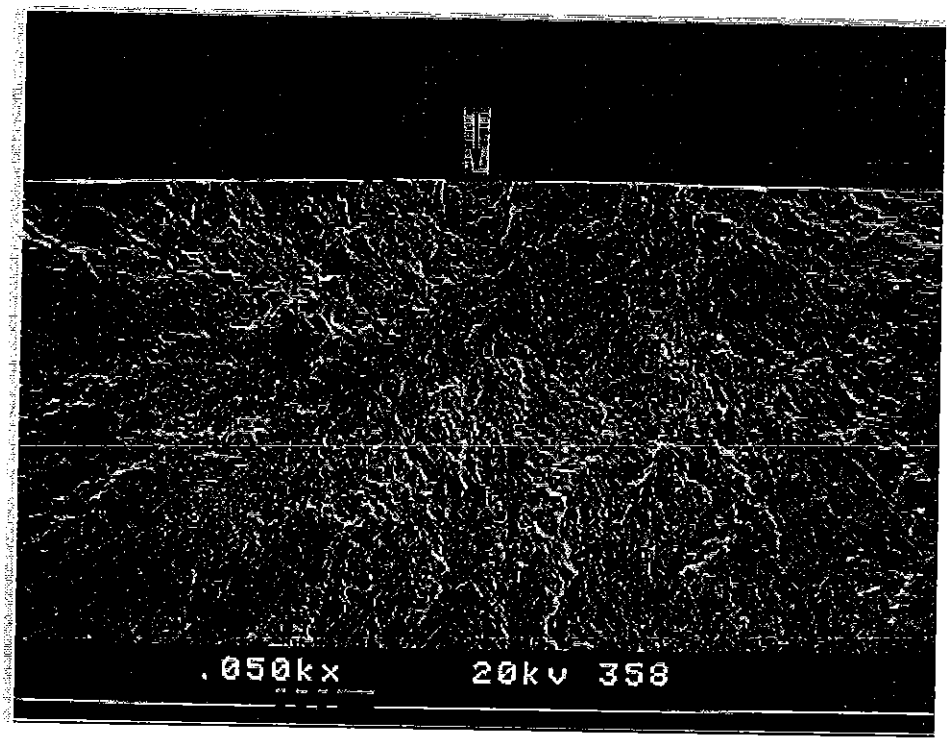

Fig. 14a Fracture region of Ti-6242 plate material (spec 3x3 in (7.6x7.6 cm). Crack initiation site and river markings are shown (P_{max} = 2600 lb (11564 N), ε_i = 6956 με, N_f = 168,229)

For a 3x2 in (7.6x5.0 cm) specimen subjected to a maximum load of 2,000 lb (8,896 N) with a yield load of 1,888 lb (8,397 N), and a maximum strain of 0.7%, the fracture surface showed a semielliptical crack initiation site where a = 0.001 in (0.003 cm) and ΔK = 8 Ksi $\sqrt{in}$ (9 MPa $\sqrt{m}$) as shown in Figure 15. Below the initiation site, striations were superimposed on facets as shown in Figure 16.

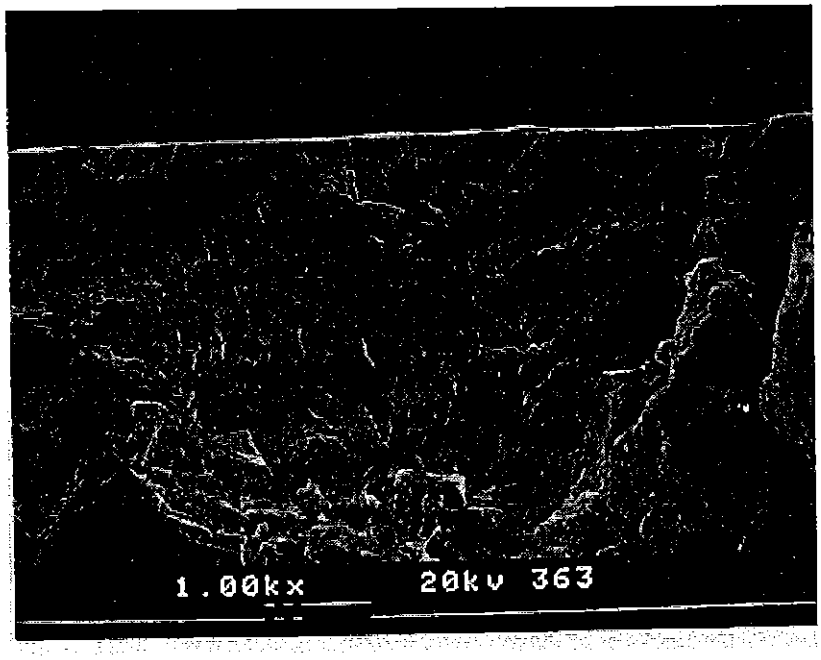

Fig. 14b Fractograph showing details of crack initiation site (spec 3x3 (7.6x7.6 cm)). Transgranular facets and tearing are shown (P_{max} = 2600 lb (11564 N), ΔK = 8 MPa $\sqrt{m}$, ε_t = 6956 $\mu\varepsilon$, N_f = 168,229)

The fracture surface of a 3x1.5 in (7.6x3.8 cm) specimen cycled at a maximum load of 1,400 lb (6,227 N) and maximum strain of 0.6% with a yield load of 1,583 lb (7,041 N) is shown in Figure 17a. At the initiation region (Figure 17b), the surface possessed facets and tear ridges where the crack had a depth of 0.004 in (0.01 cm) and ΔK = 11 Ksi $\sqrt{in}$ (12 MPa $\sqrt{m}$). As the crack grew to a depth of 0.06 in (0.15 cm), ΔK = 32 Ksi $\sqrt{in}$ (35 MPa $\sqrt{m}$), the fracture surface below the initiation site showed distinct striations (Figure 18).

The microscopic features of the fracture surfaces showed that for this material there is a dividing region where cracks at the low intensity factor, below 15 Ksi $\sqrt{in}$ (17

MPa $\sqrt{m}$), fatigue striations were absent; and the fracture surfaces were composed of long cleavage facets intermixed with poorly developed dimples. However, at higher ΔK = 25-33 Ksi $\sqrt{in}$ (28-36 MPa $\sqrt{m}$), the number of cleavage facets diminished and were replaced by dimples and fatigue striations. It is evident from the failure modes due to the magnitude of biaxial stress cycling, the fracture surfaces changed from large transgranular facets as the stress intensity is increased to more ductile fracture resulting in intergranular facets and dimples.

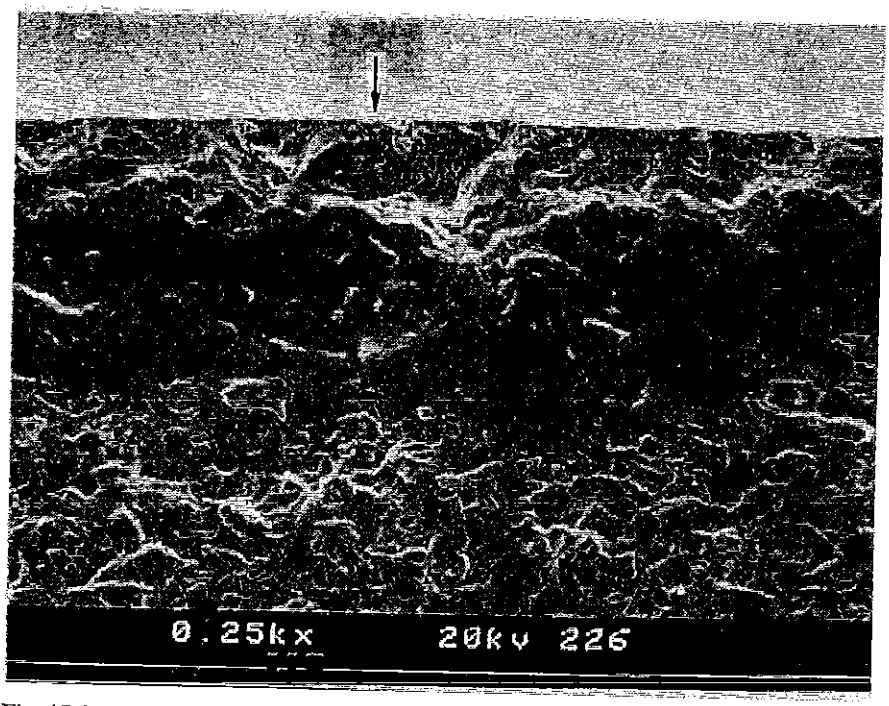

Fig. 15 Fracture region shown at top edge of fractograph (spec 3x2 in (7.6x5.0 cm)). Semielliptical initiation site is present in top surface quadrant III_T. (P_{max} = 2000 lb (8896 N), ε_1 = 7070 $\mu\varepsilon$, N_f = 151,881)

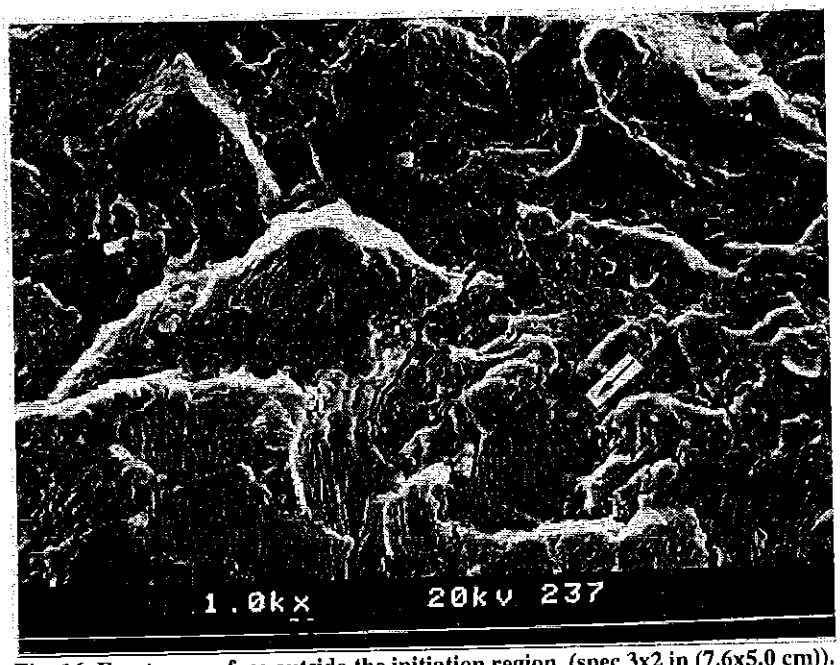

Fig. 16 Fracture surface outside the initiation region (spec 3x2 in (7.6x5.0 cm)). Transgranular facets with striations and extensive secondary cracking (P_{max} = 2000 lb (8896 N), ΔK =8 Ksi $\sqrt{in}$ (9 MPa $\sqrt{m}$), ε_1 = 7070 με, N_f = 151,881)

Fig. 17a Fracture region with semielliptical crack initiation. Initiation located in quadrant IV_T (spec 3x1.5 in (7.6x3.8 cm)) (P_{max} = 1400 lb (6227 N), ε_1 = 6082 με, N_f =286,270)

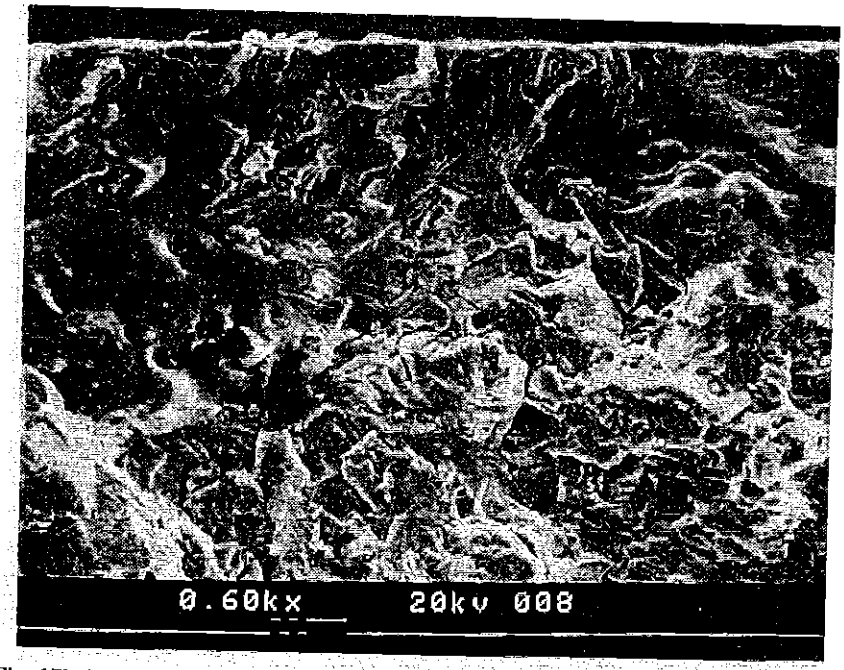

Fig. 17b Fracture surface at center of semielliptical crack initiation. (spec 3x1.5 in (7.6x3.8 cm)) (P_{max} = 1400 lb (6227 N), ΔK = 12 MPa $\sqrt{m}$, ε_1 = 6082 $\mu\varepsilon$, N_f = 286,270)

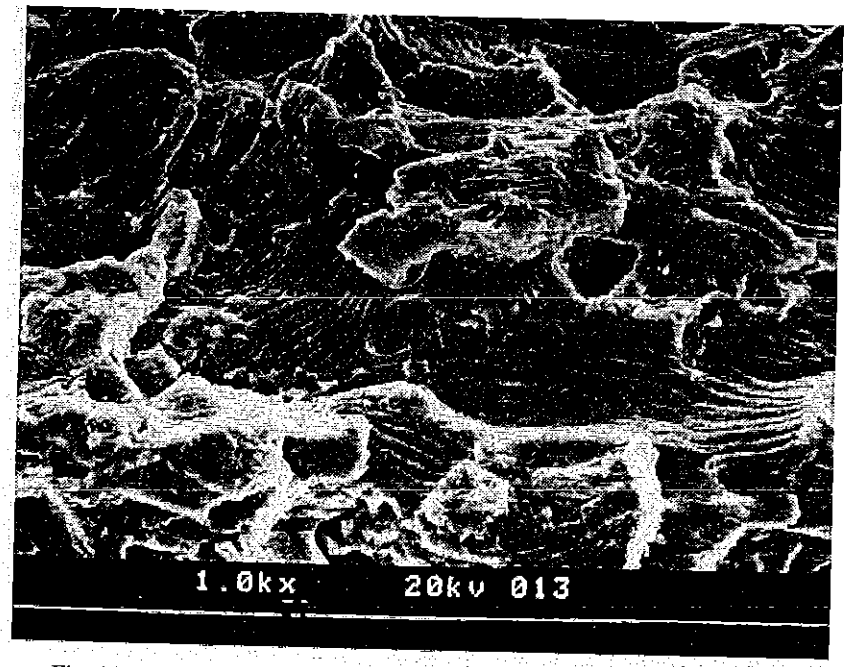

Fig. 18 Details of fracture surface below semielliptical crack initiation. Striations on facets intermixed with tearing (P_{max} = 1400 lb (6227 N), K = 35 MPa $\sqrt{m}$, ε_1 = 6082 $\mu\varepsilon$, N_f = 286,270)

Summary and Conclusions

Fatigue failure characteristics of Titanium alloy type 6Al-2Sn-4Zr-2Mo forged plate material were investigated under biaxial stress field. Anticlastic bending of plate specimens of three types of geometry were used to impose a biaxial stress field across the surface of the plate specimen with principal stress ratios of -1, - 0.44, and - 0.25 and corresponding biaxial strain ratios of -1, - 0.68, and - 0.54. The material showed a transition between transgranular and intergranular cracking depending on the magnitude of the stress intensity factor where the transition is about 15 Ksi $\sqrt{in}$ (17 MPa $\sqrt{m}$).

The biaxial fatigue test results from the 3x3 in (7.6x7.6 cm), 3x2 in (7.6x5.0 cm), and 3x1.5 in (7.6x3.8 cm) rhombic plate series were plotted in terms of maximum shear strain, maximum principal strain and von Mises effective strain versus number of cycles to failure. Although the scatter band is wider than desired, the von Mises has shown a better correlation for plate bending.

References

(1) Tor, S.S., Ruzek, J. M. and Stout, R.D., (1952), "Repeated Load Tests on Welded and Prestrained Steels," The Welding Journal, vol.31, no.5, pp.238-246-S.

(2) Zamrik, S. Y. and Davis, D. C., (1993), "A Simple Test Method and Apparatus for Biaxial Fatigue and Crack Growth Studies," Advances in Multiaxial Fatigue, ASTM STP 1191, pp.204-219.

(3) Zamrik, S. Y. and Shabara, M., (1977), "The Effect of Stress Ratio on Fatigue Crack Growth in a Biaxial Stress Field," ASME Trans., Journal of Pressure Vessel Technology, vol.99, Series J, no.1, pp.137-145.

(4) Ives, K. D., Kooistra, L. F. and Tucker, J. T., (1966), "Equibiaxial Low Cycle Fatigue Properties of Typical Pressure Vessel Steels," Journal of Basic Engineering, ASME Trans., Dec. 1966, pp.745-754.

(5) Joshi, S. R. and Shewchuk, J., (1970), "Fatigue Crack Propagation in a Biaxial Stress Field," Experimental Mechanics, vol.10, no.12, pp.529-533.

(6) Kibler, J. J. and Roberts, R., (1970), "The Effect of Biaxial Stresses on Fatigue and Fracture," Journal of Engineering Industry, ASME Trans., Series B, Nov. 1970, pp.727-734.

(7) Shewchuk, J., Zamrik, S. and Marin, J., (1968), "Low Cycle Fatigue of 7075-T6 Aluminum Alloy in Biaxial Bending," Experimental Mechanics, vol.8, Nov. 1968, pp.504-512.

(8) Itoh, T., Sakane, M. and Ohnami, M., (1994), "High Temperature Multiaxial Low Cycle Fatigue Of Cruciform Specimens," Journal of Engineering Materials and Technology, ASME Trans., vol.116, Jan. 1994, pp.90-98.

(9) Zamrik, S. Y. and Ryan, R.E., (1996), "Fatigue Crack Propagation in IN 718 Material Under Biaxial Stress Bending," Advances in Fatigue Lifetime Predictive Techniques, 3rd vol., ASTM STP 1292, pp.161-187.

(10) Lefebvre, D., Chebl, C., Thibodeau, L. and Khazzari, E., (1983), "A High Strain Biaxial Testing Rig for Thin-walled Tubes under Axial Load and Pressure," Experimental Mechanics, vol.23, no.4, pp.384-392.

(11) Makinde, A., Thibodeau, L. and Neale, K. W., (1992), "Development of an Apparatus for Biaxial Testing Using Cruciform Specimens," Experimental Mechanics, vol.32, no.2, pp.138-144.

(12) Shah, R. C. and Kobayashi, A. S., (1972), "Stress Intensity Factor for an Elliptical Crack Approaching the Surface of a Plate in Bending," ASTM STP 513, pp.3-21.

Acknowledgment: The financial support of Allied-Signal Aerospace Co., Engine Division, is greatly appreciated.